JOURNAL OF SOLID STATE CHEMISTRY 135, 36–42 (1998)
ARTICLE NO. SC977587

Oxygen Nonstoichiometry, Structures, and Physical Properties of $CaVO_{3-\delta}$

I. A Series of New Oxygen-Deficient Phases

Yutaka Ueda

Materials Design and Characterization Laboratory, Institute for Solid State Physics, The University of Tokyo, Roppongi 7-22-1, Minato-ku, Tokyo 106, Japan

Received May 8, 1997; in revised form August 6, 1997; accepted August 7, 1997

Nonstoichiometric $CaVO_{3-\delta}$ with a well-controlled oxygen content was synthesized at a $\delta = 0.01$ step by reducing stoichiometric $CaVO_{3.00}$ using a Zr sheet, and the relations between oxygen deficiency and structure were investigated. Three new phases, phase A ($0.04 < \delta < 0.08$), phase B ($\delta = 0.14$), and phase C ($\delta = 0.2$), appear in the sequence of δ's. Each phase has a vacancy-ordered structure with a much larger unit cell than the primitive one. These oxygen-deficient phases are unstable in air at room temperature and are easily oxidized to stoichiometric $CaVO_{3.00}$. All of the phases are metallic but magnetic susceptibilities of phases B and C with high oxygen deficiencies show Curie–Weiss behaviors, while stoichiometric $CaVO_{3.00}$ and phase A are Pauli paramagnets. In phases B and C there exist at least two distinct V sites in electronic state, that is, localized V sites with $S = \frac{1}{2}$ and itinerant V sites.

1. INTRODUCTION

There are many transition metal oxides with the perovskite structure or its modification. Some of these oxides exhibit a wide range of oxygen nonstoichiometry, which partly results from the characteristic that transition metals can take various valence states. Oxygen nonstoichiometry significantly affects not only the structures but also the electronic states of these compounds. Since the discovery of high-T_c superconductors, oxygen nonstoichiometry in the cuprate oxides has been extensively studied in relationship to their superconducting properties. The best known example is $YBa_2Cu_3O_y$. The oxygen nonstoichiometry in $YBa_2Cu_3O_y$ has been studied under various partial oxygen pressures (1). In this case, the holes are doped owing to oxygen nonstoichiometry and consequently the system changes from an antiferromagnetic insulator to a high-T_c superconductor with increasing doping level. The structure of $YBa_2Cu_3O_y$ changes from a tetragonal to an orthorhombic one with increasing oxygen content. The other way to control oxygen nonstoichiometry is to substitute a cation that takes a different valence state under an isostatic atmosphere. One example is $(La,Sr)CuO_{3-y}$ (2–5), where the charge imbalance associated with the substitution of Sr^{2+} for La^{3+} is compensated not by changing the valence state of copper ions but by changing the oxygen content. In these compounds, the oxygen vacancies produced in the structure are distributed in an ordered manner which results in a characteristic oxygen-deficient structure.

Compared with Cu, Fe, or Mn oxides, the study of oxygen nonstoichiometry has been scarce in the light transition metal (Ti, V, Cr) perovskite oxides. One reason for this is that extremely low partial oxygen pressures must be used to investigate the relationship between oxygen content and the atmosphere in these oxides. $SrVO_3$ and $CaVO_3$ are typical of the few known metallic perovskite oxides except high-T_c cuprates and their related oxides. It is very interesting how oxygen nonstoichiometry affects the structures and electronic states of these metallic oxides.

The oxygen nonstoichiometric compound $CaVO_{3-\delta}$ was first reported by researchers at the Electrotechnical Laboratory, Tsukuba, Japan, and subsequently has been studied by the same group. Iga and Nishihara prepared $CaVO_{3-\delta}$ with $\delta = 0.1$–0.3 by a solid-state reaction of $CaCO_3$ and VO_2 in a reducing atmosphere (pure Ar or Ar mixed with 5% H_2) (6). They also reported a metal–insulator transition caused by oxidation of the reduced samples to the stoichiometric ones (6). Thereafter, Inoue *et al.* of the same group reported that stoichiometric $CaVO_{3.0}$ is metallic and that slightly oxidized $CaVO_{3.05}$ is an insulator (7). All of the compounds have been reported to have the same orthorhombic structure ($GdFeO_3$ type). Recently, Shirakawa *et al.* of the same group reported that the X-ray diffraction pattern of $CaVO_{2.8}$ can be indexed in a monoclinic unit cell (8).

As just mentioned, the data reported on $CaVO_{3-\delta}$ are complicated and scattered over various oxygen nonstoichiometries and structures even though the data have originated from the same group. One reason for this is that it is difficult to systematically control oxygen nonstoichiometry during synthesis. Another reason is the rough

0022-4596/98 $25.00

estimation of oxygen content and insufficient identification of the structures and impurity phases. The phase relationships of $CaVO_{3-\delta}$ have not yet been established. In the present study, the oxygen nonstoichiometry of $CaVO_3$ has been well controlled by a method in which oxygen atoms are removed from the solid sample by using a Zr metal sheet, and the phase relationships and structures have been carefully investigated. As a result, a series of new oxygen-deficient compounds with vacancy-ordered structures have been found. In this paper, the relationship between oxygen deficiency and structural and physical properties in $CaVO_{3-\delta}$ are reported.

2. EXPERIMENTAL

Pure $CaVO_3$ could not be prepared by a solid-state reaction of a mixture with a stoichiometric ratio of CaO and $VO_2(V_2O_3 + V_2O_5)$. The products always contained unknown phases together with $CaVO_{3-\delta}$. However, a pure sample with a slight oxygen deficiency was successfully prepared by a solid-state reaction of an appropriate mixture of CaO, V_2O_3, and V_2O_5 in an evacuated silica tube at 600°C for 3 days and then at 1000°C for 7 days with one intermediate grinding. The stoichiometric $CaVO_{3.00}$ was prepared by annealing this oxygen-deficient sample at 120°C for several hours in air under which conditions the nonstoichiometric $CaVO_{3-\delta}$ was easily oxidized just to the stoichiometric $CaVO_{3.00}$, as described in the following section. Arc-melting of a mixture of CaO and VO_2 also gave pure $CaVO_3$, but the samples prepared by the aforementioned solid-state reaction were used in the following experiments because they were easily oxidized/reduced. In the present experiments, CaO was obtained by decomposing $CaCO_3$ at 1000°C for 1 day and then cooling it in a vacuum, and it was kept in a drybox without being exposed to the air. The starting materials V_2O_3 and V_2O_5 were obtained by reducing NH_4VO_3 in H_2 gas at 900°C for 2 days and by decomposing it in O_2 gas at 600°C for 2 days, respectively. CaO, V_2O_3, and V_2O_5 were mixed and pelletized in a drybox.

Powdered nonstoichiometric $CaVO_{3-\delta}$ with a well-controlled oxygen content was synthesized at a $\delta = 0.01$ step by reducing the stoichiometric $CaVO_{3.00}$ using a Zr sheet according to the following reaction:

$$CaVO_3 + \delta/2\,Zr \rightarrow CaVO_{3-\delta} + \delta/2\,ZrO_2$$

The weighed $CaVO_{3.00}$ was put into a gold tube and then sealed into an evacuated quartz tube together with the weighed Zr sheet, where $CaVO_3$ and the Zr sheet were seperated by a gold tube inside and outside, respectively. The reaction was carried out at temperatures between 720 and 1000°C. Hereafter this method will be called the "Zr-getting method." The detailed conditions of the reaction will be described in Section 3-2. The oxygen content of $CaVO_{3-\delta}$ was doubly checked by weighing ZrO_2 after the reaction and by thermogravimetric analysis, as described in Section 3-1.

Thermogravimetric and differential thermal analysis (TG-DTA) measurements were performed with a Mac Science TG-DTA 2000 system both to determine oxygen content and to examine oxidation processes.

The obtained samples were carefully examined to include no impurity phase and also characterized by powder X-ray diffraction using a Mac Science MXP[18] system with a rotating-anode generator and a monochromator of single-crystalline graphite for Cu$K\alpha$ radiation.

Magnetic susceptibility was measured using a SQUID magnetometer in the temperature range 5–700 K at an applied magnetic field of 1T. The sample was sealed into a quartz capillary with He gas to avoid oxidation during the measurements.

3. RESULTS AND DISCUSSION

3-1. Thermogravimetric and Differential Thermal Analysis (TG-DTA)

Figure 1 shows TG-DTA curves for the nonstoichiometric sample on heating at 5°C/min in air. The weight increases stepwise accompanied by exothermic peaks in the DTA curve; that is, on heating, the oxidation gradually starts just from room temperature, rapidly progresses around 120°C, showing an exothermic peak in the DTA curve, ends around 150°C, and then does not progress in the temperature range between 150 and 400°C (the first step). The next process of oxidation starts above 400°C and ends around 700°C (the final step), showing a broad exothermic peak in the DTA curve. As the final product was identified to be $CaVO_{3.5}(Ca_2V_2O_7)$, the oxygen contents at the first

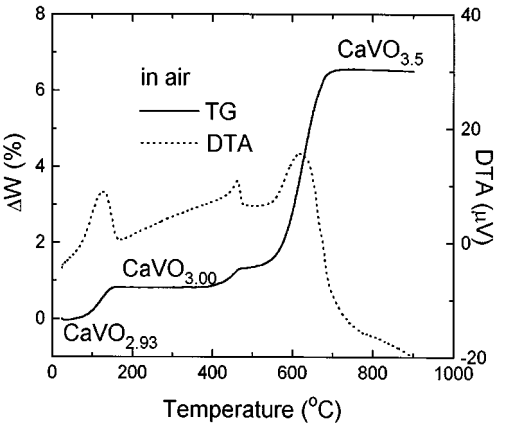

FIG. 1. TG-DTA curves for $CaVO_{3-\delta}$ heated in air. Oxygen content was determined from the weight difference between each step and the final state, $CaVO_{3.5}(Ca_2V_2O_7)$.

step and the initial state were estimated from the amount of weight gain to be 3.00 ± 0.002 and 2.93 ± 0.002, respectively. TG-DTA curves for the stoichiometric $CaVO_{3.00}$ were the same as those for the nonstoichiometric $CaVO_{3-\delta}$ except for the absence of the first oxidation process below 150°C. From the TG-DTA experiments, it was confirmed that the nonstoichiometric $CaVO_{3-\delta}$ is easily oxidized just to the stoichiometric $CaVO_{3.00}$ below 150°C in air and the stoichiometric $CaVO_{3.00}$ is stable up to about 400°C. In the following experiments, the oxygen content of nonstoichiometric $CaVO_{3-\delta}$ prepared by the Zr-getting method was determined by measuring the weight gain from the initial state to the first step ($CaVO_{3.00}$) in the TG curve, which was in excellent agreement with the value calculated from the weight of ZrO_2.

In addition to these steps, an anomalous step was always observed around 450°C and $\delta \approx -0.05$ in the TG curve accompanied by a small exothermic peak in the DTA curve, as can be seen in Fig. 1. A similar anomaly in the TG curve was reported by Inoue *et al.* (7). They reported a metal–insulator transition in the compound at the step. In the present experiments, the resistivity of the sintered sample cooled from 450°C showed an insulating behavior, in agreement with the previous report (7), although it showed the same X-ray diffraction pattern as that of stoichiometric $CaVO_{3.00}$, which was consistent with the results of NMR experiments (9). The metallic behavior, however, was recovered by regrinding and subsequently repressing the sample at room temperature. This suggests that the surface of the particles of the cooled sample is covered by a thin film of an insulating compound. However, the oxidation of the surface of the particles does not seem to explain this anomalous behavior in the TG-DTA curve. Further investigation will be necessary to elucidate the mechanism of the oxidation.

3-2. Phase Relations and Oxygen Contents

As already described in Section 3-1, the reduced samples were oxidized even at room temperature in air. Therefore X-ray diffraction measurements for the reduced samples were carried out under vacuum ($\sim 10^{-3}$ Torr) at room temperature using an apparatus for high-temperature X-ray diffraction measurements to prevent the samples from oxidizing during the measurement. The powder X-ray diffraction patterns of the $CaVO_{3-\delta}$ samples reduced above 900°C showed a systematic change with increasing δ in the composition range $0 < \delta < 0.1$ but in the range $\delta \geq 0.1$, they were similar to those of the less reduced ($\delta < 0.1$) samples. From careful analysis of the X-ray diffraction patterns, it was confirmed that a small amount of $CaVO_{2.5}$ ($CaV_2O_4 + CaO$) coexists with $CaVO_{3-\delta}$ in such samples; that is, a part of $CaVO_{3-\delta}$ was decomposed into CaV_2O_4 and CaO under the conditions of 900°C and $\delta \geq 0.1$ and consequently the less reduced $CaVO_{3-\delta}$ was produced as a main phase. The reaction below 720°C was necessary for preparing pure $CaVO_{3-\delta}$ with $\delta \geq 0.1$. However, it was impossible to reduce the samples beyond $y = 0.22$ at 720°C even after 1 month. In the present study, the phase relationships in $CaVO_{3-\delta}$ could be determined in the nonstoichiometric region of $0 \leq \delta \leq 0.2$. Figure 2 shows portions of X-ray diffraction patterns of $CaVO_{3-\delta}$ collected for a sequence of δ's, where the contribution of Cu$K\alpha_2$ is arithmetically subtracted. It can be clearly seen in Fig. 2 that four phases appear across the coexistence of each phase in the sequence of δ's. The obtained phase relation is shown in Table 1 together with the reaction conditions. The orthorhombic phase with the $GdFeO_3$-type structure exists only at the stoichiometric composition, and a very slight oxygen deficiency results in the coexistence with the unknown phase A. Phase A appears in the narrow region of $0.04 < \delta < 0.08$ as a single phase. With further increasing δ, the unknown phases B and C appear around $\delta = 0.14$ and 0.2, respectively. Phases B and C show slight oxygen nonstoichiometry. Above $\delta = 0.2$, $CaVO_{2.5}$($CaV_2O_4 + CaO$) coexisted with phase C.

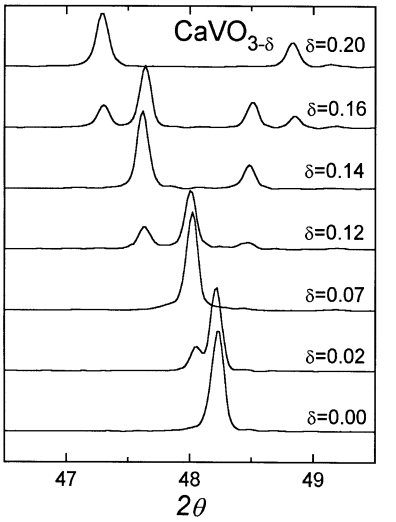

FIG. 2. Portions of powder X-ray diffraction patterns of $CaVO_{3-\delta}$ collected for the sequence of δ's. The contribution of Cu$K\alpha_2$ is arithmetically subtracted.

TABLE 1
Phases in $CaVO_{3-\delta}$

Compound	δ	Conditions
$GdFeO_3$ type	$\delta = 0.00$	
Phase A	$0.04 < \delta < 0.08$	$T \sim 900$°C, 4 days
Phase B	$\delta = 0.14$	$T \leq 720$°C, 2 weeks
Phase C	$\delta = 0.2$	$T \leq 720$°C, 2 weeks

3-3. X-ray Diffraction Patterns

The X-ray diffraction patterns of the four phases in $CaVO_{3-\delta}$ are shown in Fig. 3 together with that (Fig. 3a) of the cubic perovskite $SrVO_3$ for reference. The raw X-ray diffraction data without subtraction of the contribution of $CuK\alpha_2$ are shown in Fig. 3. Clear reflections from $CuK\alpha_2$ can be seen above a rather low 2θ. This indicates that the obtained samples are very homogeneous and have a good crystallization. The X-ray diffraction pattern (Fig. 3b) for the stoichiometric $CaVO_{3.00}$ is of a typical orthorhombic $GdFeO_3$-type structure with $a, b \approx \sqrt{2}a_p$ and $c \approx 2a_p$, where a_p is the a parameter of cubic perovskite. All Bragg reflections can be indexed in an orthorhombic cell with $a = 0.5317(6)$ nm, $b = 0.5341(5)$ nm, and $c = 0.7545(5)$ nm, as shown in Fig. 3b. The X-ray diffraction pattern (Fig. 3c) of phase A is very similar to that of $SrVO_3$, that is, a cubic perovskite. In phase A, the main reflections referred to the Bragg peaks of $SrVO_3$ are very sharp with no splitting, indicating no distortion of the lattice, and they can be indexed in a cubic unit cell with $a = 0.3786(3)$ nm, as shown in Fig. 3c. In addition to these main reflections, however, there exist many extra reflections with weak intensity that cannot be indexed in any cubic cell. These extra reflections are essential for phase A because they vanish in the oxidation of phase A to the stoichiometric $CaVO_{3.00}$ at 120°C in air. If they had originated in an impurity phase such as CaV_2O_4, they would have remained in the oxidation at such a low temperature; for instance, CaV_2O_4 appeared in the samples reduced above 720°C and coexisted with the stoichiometric $CaVO_{3.00}$ after the oxidation. The reflections observed in the low 2θ region which are shown in the inset of Fig. 3c indicate a much larger supercell than the primitive cubic cell. As described in Section 3-2, this phase has the nonstoichiometric region of $0.04 < \delta < 0.08$. The compositional dependence of the extra reflections is strange in the d-value (or 2θ) as shown in Fig. 4. The main reflections shift to the lower 2θ side with increasing δ, indicating an expansion of the lattice with increasing δ, but the additional reflections, for example, the x and y in Fig. 4, shift in opposite directions (to the lower 2θ side for the x and to the higher 2θ side for the y). Such behavior for extra reflections has been often observed in the X-ray diffraction of compounds with modulated structures. These results suggest a vacancy-ordered structure with a modulated lattice as a plausible structure for phase A.

Figures 3d and 3e show the X-ray diffraction patterns for phases B and C, respectively. In these patterns, the main reflections split into two or three peaks, suggesting an

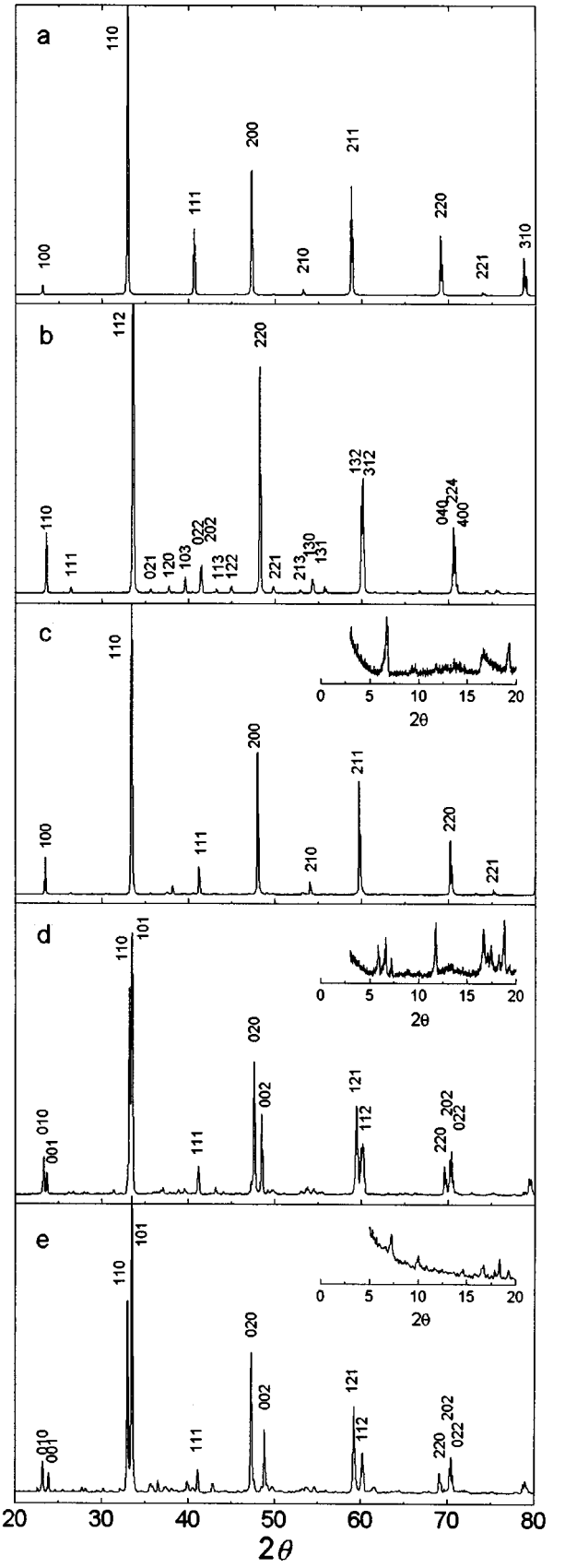

FIG. 3. X-ray diffraction patterns for (a) $SrVO_3$, (b) $CaVO_{3.00}$, (c) phase A, (d) phase B, and (e) phase C. X-ray diffraction patterns below $2\theta = 20°$ are shown in the insets for phases A, B, and C.

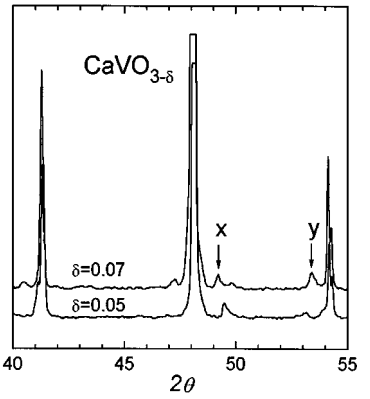

FIG. 4. Portions of powder X-ray diffraction patterns of $CaVO_{3-\delta}$ with $\delta = 0.05$ and 0.07. The x and y represent the extra reflections with weak intensity which originate in a vacancy-ordered structure with a larger unit cell than that of the primitive one.

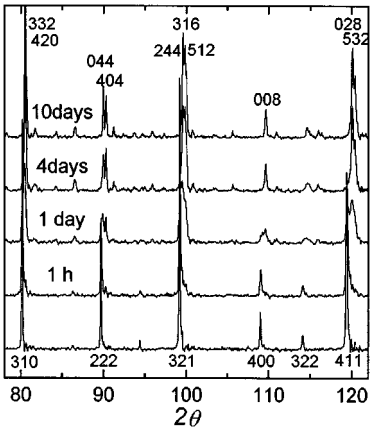

FIG. 5. X-ray diffraction patterns as a function of time for which $CaVO_{3-\delta}$ with $\delta = 0.07$ (phase A) was left in air at room temperature. The X-ray diffraction pattern changes from a cubic (bottom figure) to an orthorhombic one (top figure).

orthorhombic (pseudotetragonal) or a monoclinic distortion of the primitive lattice. Actually, the main reflections can be indexed in orthorhombic cells with $a = 0.3822(4)$ nm, $b = 0.3811(9)$ nm, and $c = 0.3751(5)$ nm for phase B and $a = 0.3841(7)$ nm, $b = 0.3837(4)$ nm, and $c = 0.3726(1)$ nm for phase C, respectively, as shown in Figs. 3d and 3e. The X-ray diffraction pattern for phase C is similar to that of $CaVO_{2.8}$ previously reported by Shirakawa *et al.* (8). They proposed a monoclinic cell with lattice parameters $a = 0.5382(5)$ nm, $b = 0.7499(1)$ nm, $c = 0.5388(7)$ nm and $\gamma = 90.22(7)^\circ$ based on the $GdFeO_3$-type structure. Also in phases B and C many extra reflections with weak intensity are observable in addition to the main reflections, as can be seen in Figs. 3d and 3e. These extra reflections were not reported by Shirakawa *et al.* (8). The existence of extra reflections in the low 2θ region suggests a vacancy-ordered structure with a larger unit cell. A series of superspots that are equally divided by 15 (phase B) or 20 times (phase C) between the main spots has been observed in preliminary electron diffraction measurements. Such a long periodicity and a large amount of vacancies suggest an ordered arrangement of tunnel defects or planar defects as a possible vacancy-ordered structure. Planar defects (shear structure) may be ruled out in this case because planar defects of only oxygen atoms are hardly realized in the perovskite structure. A study of the precise crystal structure is now in progress by electron microscopy, which is well known to be the most useful tool for investigation of vacancy-ordered manner.

3-4. Reactivity at Room Temperature

The stoichiometric $CaVO_{3.00}$ with $GdFeO_3$-type structure is very stable at room temperature in air while the nonstoichiometric $CaVO_{3-\delta}$ are gradually oxidized to the stoichiometric $CaVO_{3.00}$ under the same conditions. Figure 5 shows the X-ray diffraction patterns as a function of time for which the sample with $\delta = 0.07$ (phase A) was left in air at room temperature, where the contribution of Cu$K\alpha_2$ is arithmetically subtracted and the indices for the initial and final patterns are of the cubic and orthorhombic cells, respectively. The Bragg peaks of the stoichiometric compound were already recognized in the X-ray diffraction pattern taken after the sample was left in air for 1 h. The sample was perfectly oxidized to the stoichiometric $CaVO_{3.00}$ after being left in air for about 10 days in the winter. The oxidation progressed more rapidly in the summer. Phases B and C were oxidized more slowly compared with phase A. It should be noticed that it was very difficult to observe the electron diffraction pattern of phase A in the electron microscope because the sample was heated by the electron beams and immediately oxidized even in such a high vacuum (1×10^{-8} Torr).

3-5. Magnetic Properties

The magnetic susceptibilities (χ) of $CaVO_{3-\delta}$ with $\delta = 0$, 0.05, 0.07, 0.14, and 0.2 are shown in Fig. 6. Both the stoichiometric $CaVO_{3.00}$ and phase A ($\delta = 0.05$ and 0.07) show Pauli paramagnetic behaviors which are reasonable for their metallic properties. The absolute value of χ increases in proportion to δ. This suggests an increase in the number of carriers or density of states with increasing δ. On the other hand, the χ of phases B and C show Curie–Weiss behaviors, $\chi = C/(T - \Theta) + \chi_0$, although both phases are also metallic. The Curie constant (C), Weiss temperature (Θ), and temperature-independent term (χ_0) of the magnetic susceptibility for each phase are shown in the inset of Fig. 6. It was impossible to explain the temperature dependence of χ for phase C by fixed parameters in the

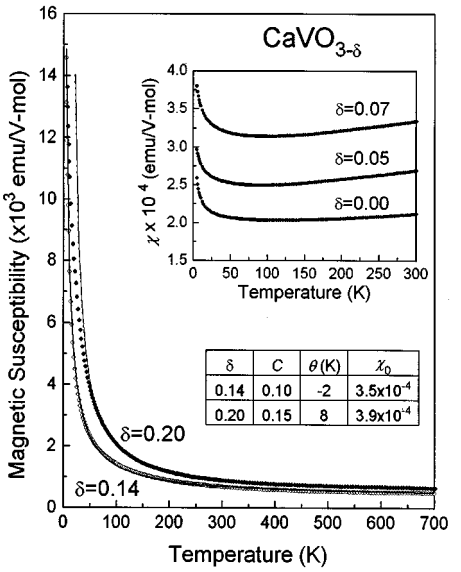

FIG. 6. Temperature dependence of the magnetic susceptibilities of $CaVO_{3-\delta}$ with $\delta = 0$, 0.05, 0.07, 0.14, and 0.20. The solid lines represent the Curie–Weiss fittings. The Curie constant (C), Weiss temperature (Θ), and temperature-independent term of the magnetic susceptibility (χ_0) are shown in the inset for $CaVO_{3-\delta}$ with $\delta = 0.14$ and 0.20.

whole temperature region measured. Since the fit of χ below 300 K to a Curie–Weiss law gave a meaningless negative χ_0, the Curie–Weiss fitting was done above 50 K, as shown by the solid line in Fig. 6. The observed χ deviates from the Curie–Weiss law below about 50 K. The obtained Curie constant corresponds to a concentration of 27% for the localized spin with $S = \frac{1}{2}$ or 10% for that with $S = 1$ in phase B, while it corresponds to 40% for $S = \frac{1}{2}$ or 15% for $S = 1$ in phase C. On the basis of an ionic model, $CaVO_{3-\delta}$ can be regarded as a mixed-valence oxide consisting of $100(1-2\delta)\%V^{4+}$ (matrix) and $200\delta\%V^{3+}$. If V^{3+} (d^2, $S = 1$), associated with oxygen deficiency, behaves as a localized spin with $S = 1$ in the delocalized matrix, the concentration of the localized spin can be estimated to be 28% in phase B ($\delta = 0.14$) and 40% in phase C ($\delta = 0.2$), respectively. These values are much larger than those (10% for phase B and 15% for phase C) obtained from the Curie constants. The oxygen deficiency produces two electrons per oxygen vacancy and they may behave as a localized impurity with $S = \frac{1}{2}$. In this case, the Curie constants for phases B and C are calculated to be 0.10 and 0.15, respectively. The calculated values for phases B and C are just equal to the observed values, 0.10 and 0.15, respectively.

Apart from the discussion on the origin of localized spins, these results indicate that there exist at least two distinct V sites, that is, delocalized and localized V sites, both in phases B and C. One can refer to nonstoichiometric compounds V_2O_{3+x} (or $V_{2-y}O_3$) (10, 11) or Magnéli phase vanadium oxides (12, 13) as metallic vanadium oxides in which magnetic susceptibilities show Curie–Weiss behaviors. In V_2O_{3+x}, V^{4+}-like sites associated with the nonstoichiometry behave as a localized impurity in the almost delocalized majority V sites (10, 11). In the metallic phase of Magnéli phase vanadium oxides, there exist at least three distinct V sites which show independent Curie–Weiss behaviors (12, 13). The origin of Curie–Weiss behaviors in these metallic compounds is a current topic in highly correlated electronic systems. Phases B and C may be situated in such a highly correlated electronic system. In $CaVO_{3-\delta}$, the electron correlation becomes strong with increasing δ and a high oxygen deficiency leads to a charge differentiation, that is, V sites with the localized spin near the oxygen vacancies and delocalized V sites far from the oxygen vacancies, although the system remains metallic. It should be noticed that the color of $CaVO_{3-\delta}$ changes from blue-black in $CaVO_{3.00}$ and phase A to black in phases B and C. In the metallic vanadium oxides, metallic antiferromagnetic states often appear as ground states but no evidence for a magnetic order or spin-glass state has been observed in phases B and C. The study of the microscopic electronic state of $CaVO_{3-\delta}$ is now in progress by ^{51}V NMR.

4. SUMMARY

The nonstoichiometric $CaVO_{3-\delta}$ with a well-controlled oxygen content was synthesized at a $\delta = 0.01$ step by reducing the stoichiometric $CaVO_{3.00}$ using a Zr sheet, and the relations between oxygen deficiency and structure were investigated. Three new phases, phase A ($0.04 < \delta < 0.08$), phase B ($\delta = 0.14$), and phase C ($\delta = 0.2$), appear in the sequence of δ's. Each phase has a vacancy-ordered structure with a much larger unit cell than the primitive one. A modulated structure for phase A and an ordered arrangement of tunnel defects for phases B and C are proposed as plausible vacancy-ordered structures from the results of powder X-ray diffraction. These oxygen-deficient phases are unstable in air at room temperature and are easily oxidized to the stoichiometric $CaVO_{3.00}$. All of the phases are metallic but the magnetic susceptibilities of phases B and C with high oxygen deficiencies show Curie–Weiss behaviors, while the stoichiometric $CaVO_{3.00}$ and phase A are Pauli paramagnets. In phases B and C there exist at least two distinct V sites in the electronic state, that is, localized V sites with $S = \frac{1}{2}$ and itinerant V sites.

ACKNOWLEDGMENTS

The author thanks Prof. N. Nakayama (Yamaguchi University) for preliminary electron diffraction measurements. This work was supported by a Grant-in-Aid for Scientific Research from the Ministry of Education, Science, Sports and Culture.

REFERENCES

1. For example: K. Kishio, J. Shimoyama, T. Hasegawa, K. Kitazawa, and K. Fueki, *Jpn. J. Appl. Phys.* **26,** L1228 (1987).
2. K. Otzschi, A. Hayashi, Y. Fujiwara, and Y. Ueda, *J. Solid State Chem.* **105,** 573 (1993).
3. K. Otzschi and Y. Ueda, *J. Solid State Chem.* **107,** 149 (1993).
4. K. Otzschi, A. Hayashi, and Y. Ueda, *J. Supercond.* **7,** 73 (1994).
5. K. Otzschi, K. Koga, and Y. Ueda, *J. Solid State Chem.* **115,** 490 (1995).
6. F. Iga and Y. Nishihara, *J. Phys. Soc. Jpn.* **61,** 1867 (1992).
7. H. Inoue, K. Morikawa, H. Fukuchi, T. Tsujii, F. Iga, and Y. Nishihara, *Physica B* **194–196,** 1067 (1994).
8. N. Shirakawa, K. Murata, H. Makino, F. Iga, and Y. Nishihara, *J. Phys. Soc. Jpn.* **64,** 4824 (1995).
9. H. Nishihara, F. Iga, Y. Nishihara, T. Machida, S. Matsumoto, and Y. Nakamura, *Physica B* **194–196,** 235 (1994).
10. Y. Ueda, K. Kosuge, S. Kachi, H. Yasuoka, H. Nishihara, and A. Heidemann, *J. Phys. Chem. Solids* **39,** 1281 (1978).
11. Y. Ueda, K. Kosuge, and S. Kachi, *J. Solid State Chem.* **31,** 171 (1980).
12. A. C. Gossard, J. P. Remeika, T. M. Rice, H. Yasuoka, K. Kosuge, and S. Kachi, *Phys. Rev. B* **9,** 1230 (1974).
13. S. Kachi, Y. Ueda, and K. Kosuge, *Ferrites*, 131 (1980).